Final vibrational state resolved single-electron capture for impact of $\leqslant$ 1 keV C^{2+} on H$_2$, N$_2$, O$_2$ and CO

P Leputsch, D Dumitriu†, F Aumayr and H P Winter‡

Institut für Allgemeine Physik, Technische Universität Wien, Vienna, Austria

Abstract. By means of ion translational energy spectroscopy, single-electron capture (SEC) by ground state and metastable C^{2+} on H$_2$, N$_2$, O$_2$ and CO has been studied at impact energies $\leqslant$ 1 keV. For SEC from N$_2$ the main channels involve transitions C^{2+}(2s2p ^{3}P$^{\rm o}$) + N$_2$(v_i = 0) $\rightarrow$ C$^+$(2s2p^2 ^{2}D) + N$_2^+$(A $^2\Pi_{\rm u}$; v_f) with the final vibrational state distributions (v_f = 0–5) being found in reasonably good agreement with multichannel Landau–Zener calculations.

1. Introduction

Single-electron capture (SEC) by slow multicharged ions (MCI; in the context of this work we refer by 'slow' to impact energies of $\leqslant$ 1 keV amu^{-1}) from neutral atoms or molecules is characterized by a strong relation between the particular reaction energy defects and couplings of respective initial and final quasimolecular states which are transiently formed during the collision (Janev and Winter 1985). In order to assess the importance of SEC processes for, for example, stellar atmospheres (Heil 1987) or thermonuclear fusion edge plasmas (Janev 1995), state-to-state selective information on the relevant inelastic processes is especially important. Experimentally this can be obtained by photon spectroscopy for projectile and target states which are being excited due to SEC (e.g. Hoekstra *et al* 1991), or by means of translational energy spectroscopy of projectiles having undergone SEC (Gilbody 1994). The latter technique is considerably more sensitive and also covers SEC into ground state and long-lived excited (metastable) projectile states, but is usually subject to a poorer state resolution due to the kinetic energy spread of the projectile ions. Theoretical treatment of state-selective SEC by MCI is achieved with semiclassical or fully-quantum-mechanical methods (cf Janev *et al* 1995). However, fairly reliable estimates of the respectively dominant reaction channels can already be obtained from the classical over barrier model (e.g. Niehaus 1986) or from Landau–Zener-type calculations (e.g. Salop and Olson 1976, Kimura *et al* 1984, Taulbjerg 1986). For molecular target particles at room temperature their initial vibrational excitation can be neglected, but the influence of SEC on their ionic final vibrational state distribution is of interest. Applicability of the Franck–Condon principle to such collisions depends on the ratio of the involved collisional interaction time and molecular vibration periods. So-called 'vertical electronic transitions' via SEC from the neutral to various ionized molecular states can only be expected at sufficiently high impact energy where the initial target vibrational state stays practically frozen during the essential part of the collision (Gislason and Parlant 1987).

† Visiting Scientist from Institute of Physics and Nuclear Engineering, Bucharest, Romania.

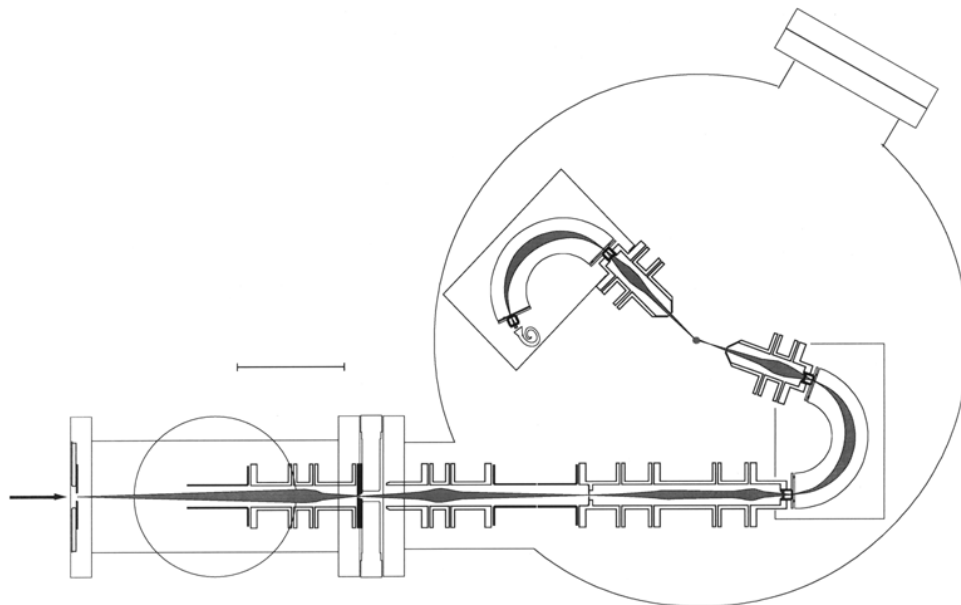‡ Author to whom correspondence should be sent. E-mail address: winter@iap.tuwien.ac.at

Figure 1. Schematic view of ion translational energy spectrometer (for details cf section 2).
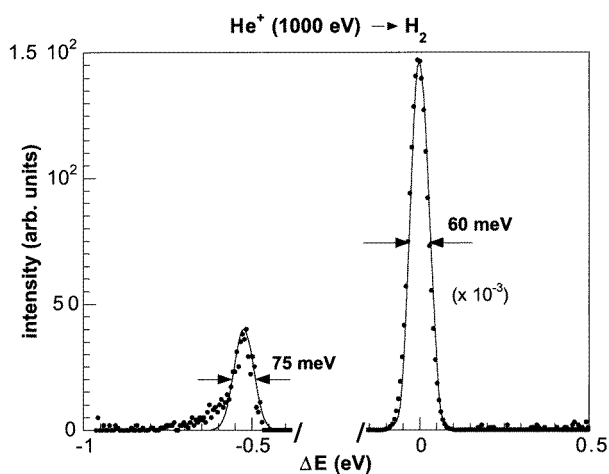

Figure 2. TES for 1 keV He^+–H_2 collisions at $\vartheta = 0°$.

Numerous groups have studied inelastic processes for impact of singly charged ions on molecules by means of translational energy spectroscopy (e.g. Kobayashi *et al* 1978, Linder 1980, Itoh *et al* 1983, Nakamura *et al* 1986, Neidner-Schatteburg and Toennies 1992, Brenton 1995).

In such studies the coverage of SEC processes requires measuring the energy loss of neutralized projectiles (e.g. Hodge *et al* 1977, Matsuo *et al* 1982), whereas for doubly or multiply charged primary ions also the charge-exchanged projectiles are still ionized. However, for studies on SEC by MCI from molecular targets by means of translational energy spectroscopy only in a few cases has final-vibrational state resolution been achieved,
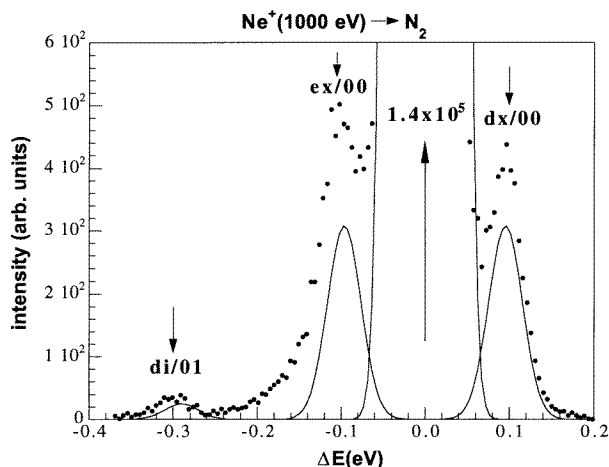
Figure 3. TES for 1 keV Ne^{+}–N_2 collisions at $\vartheta = 0°$; for further explanations cf text.

so far (Ar^{3+}, Xe^{2+}–H_2 by Huber and Kahlert (1985), Ne^{2+}–H_2 by Fukuroda *et al* (1989), Ne^{2+}–N_2 by Okuno *et al* (1989), He^{2+}–NO by Farnik *et al* (1993)). We have constructed a new translational energy spectrometer with considerably higher resolution than available in our own former studies on SEC in C^{2+}–H_2 collisions (Unterreiter *et al* 1991), whereby no final vibrational state resolution could be achieved. With this new instrument we have first investigated SEC by ground state and metastable C^{2+} from simple molecules such as H_2, N_2, O_2 and CO. In particular, for the C^{2+}–N_2 collision system the dominant SEC channel involves final vibrational state distributions in good agreement with also performed multichannel Landau–Zener calculations.

After submission of this work to *J. Phys. B* we have learnt of a recently published translational energy spectroscopy study on state-selective SEC by 4 keV ground state and metastable C^{2+} ions from H_2, N_2 and O_2 by Burns *et al* (1997). Because of the different impact energies involved, no direct comparison of their results with ours is possible, but both studies agree on the respective main SEC reaction channels. However, the energy resolution achieved by Burns *et al* (1997) does not permit the resolution of final vibrational projectile states as in the present study.

2. Experimental methods

2.1. Translational energy spectrometer

Our experimental apparatus as sketched in figure 1 consists of an ion translational energy spectrometer (Kobayashi *et al* 1978, Sato and Moore 1979, Kahlert *et al* 1983, Wilkie *et al* 1986, Schweinzer and Winter 1989, Gilbody 1994, Brenton 1995), to which primary ions are delivered either by a Nier-type ion source with variable electron impact energy (Schweinzer and Winter 1989), or a 5 GHz ECR multicharged ion source (Leitner *et al* 1994). Primary ions are accelerated to 1 keV, magnetically selected and transported via sets of electrostatic lenses and steering plates into the main collision chamber of all stainless steel construction, which is evacuated by a 500 l s^{-1} turbomolecular pump with liquid-N_2 baffle to a base pressure in the low 10^{-6} Pa region. The collision chamber houses two electrostatic 160° spherical spectrometers (comstock type AC-902) for kinetic energy definition of primary

Table 1. Approximate energy differences in eV for vibrational excitation and ionization of H_2 and N_2, and for vibrational excitation of H_2^+ and N_2^+, respectively (Herzberg 1950, Fukuroda *et al* 1989), and for O_2, O_2^+, CO, CO^+, respectively (Huber and Herzberg 1979).

Mol. state	Vibrational transitions $v' \to v''$						
	$0 \to 1$	$1 \to 2$	$2 \to 3$	$3 \to 4$	$4 \to 5$	$5 \to 6$	$6 \to 7$
$H_2(X\,^1\Sigma_g^+)$	0.52	0.49	0.46	0.43	0.40		
ionization energy to $H_2^+(X\,^2\Sigma_g^+)$ 15.43 eV, $H_2^+(B\,^2\Sigma_g^+)$ 27.06 eV.							
$H_2^+(X\,^2\Sigma_g^+)$	0.27	0.25	0.24	0.22	0.21	0.19	0.17
$H_2^+(B\,^2\Sigma_g^+)$	0.053	0.051	0.050	0.049	0.047		
$N_2(X\,^1\Sigma_g^+)$	0.29	0.29	0.28	0.28	0.27		
ionization energy to $N_2^+(X\,^2\Sigma_g^+)$ 15.58 eV, $N_2^+(A\,^2\Pi_{ui})$ 16.70 eV, $N_2^+(B\,^2\Sigma_u^+)$ 18.74 eV.							
$N_2^+(X\,^2\Sigma_g^+)$	0.27	0.27	0.26	0.26	0.25		
$N_2^+(A\,^2\Pi_{ui})$	0.23	0.23	0.22	0.22	0.22		
$N_2^+(B\,^2\Sigma_u^+)$	0.29	0.29	0.28	0.28	0.27		
$O_2(X\,^3\Sigma_g^-)$	0.19	0.19	0.19	0.18	0.18		
ionization energy to $O_2^+(X\,^2\Pi_g)$ 12.07 eV, $O_2^+(a\,^4\Pi_{ui})$ 16.10 eV, $O_2^+(A\,^2\Pi_u)$ 17.11 eV, $O_2^+(b\,^4\Sigma_g^-)$ 18.21 eV, $O_2^+(C\,^2\Phi_u)$ 18.72 eV, $O_2^+(D\,^2\Sigma_g)$ 19.85 eV, $O_2^+(B\,^2\Sigma_g^-)$ 20.43 eV, $O_2^+(c\,^4\Sigma_u^-)$ 24.58 eV.							
$O_2^+(X\,^2\Pi_g)$	0.23	0.23	0.22	0.22	0.22		
$O_2^+(a\,^4\Pi_{ui})$	0.13	0.12	0.12	0.12	0.12		
$O_2^+(A\,^2\Pi_u)$	0.11	0.10	0.10	0.10	0.09		
$O_2^+(b\,^4\Sigma_g^-)$	0.14	0.14	0.14	0.13	0.13		
$O_2^+(B\,^2\Sigma_g^-)$	0.14	0.13	0.13	0.12	0.12		
$CO(X\,^1\Sigma_g^+)$	0.27	0.26	0.26	0.26	0.25		
ionization energy to $CO^+(X\,^2\Sigma^+)$ 14.01 eV, $CO^+(A\,^2\Pi_i)$ 16.58 eV, $CO^+(B\,^2\Sigma^+)$ 19.70 eV.							
$CO^+(X\,^2\Sigma^+)$	0.27	0.27	0.26	0.26	0.26		
$CO^+(A\,^2\Pi_i)$	0.19	0.19	0.18	0.18	0.18		
$CO^+(B\,^2\Sigma^+)$	0.21	0.20	0.19	0.19	0.18		

ions (monochromator) entering the collision cell, and for kinetic energy analysis (analyser) of ions having passed the collision cell, respectively (see figure 1). The collision cell is fed by a target gas-inlet system and can be precisely aligned by a manipulator (rotation in the horizontal plane and translation in the x-, y- and z-directions). Attached to the collision cell is a small Faraday cup for convenient ion current tuning. Both the monochromator and analyser are operated in the constant pass-energy mode with typical pass energies q.e. $U_p \leqslant 10$ eV times ion charge. Before entering either of the spectrometers, ions are decelerated to their appropriate pass energy by means of three-element lenses. Primary ions leaving the monochromator are re-accelerated to a desired collision energy, and ions having passed the analyser are re-accelerated to about 2 keV for counting by a channeltron detector. The analyser can be rotated around the scattering centre to select projectile scattering angles ϑ from 90° through forward scattering ($\vartheta = 0$) until $-15°$.

All translational energy spectra (TES) to be presented have been measured at $\vartheta = 0$, by superimposing a sawtooth ramp voltage of variable amplitude on the deceleration potential of the analyser entrance lens, which is connected to the analyser bias by a fixed voltage according to the impact energy chosen.
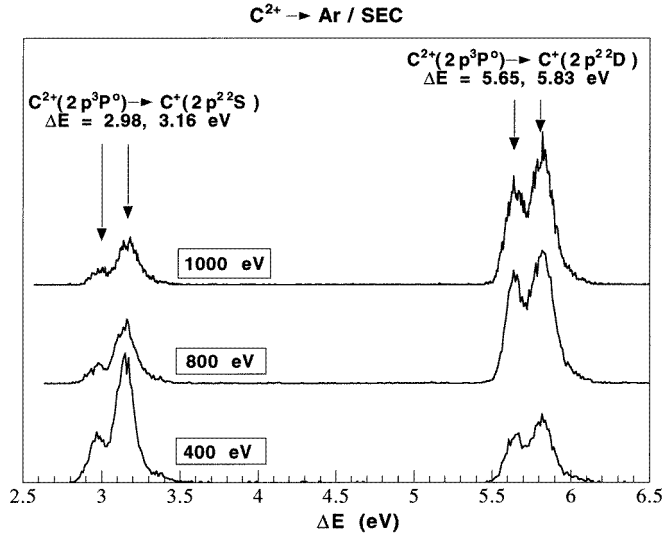
Figure 4. Main TES peaks for SEC in C^{2+}–Ar collisions ($E = 1, 0.8, 0.4$ keV; $\vartheta = 0°$).

Table 2. Configurations and excitation energies of C^+ ground state and five lowest excited states, and ionization energies for C^{2+} ground state and metastable state from C^+ ground state (fine structure splittings neglected; compiled from Bashkin and Stoner (1975)).

Ion	Configuration	Excitation/ionization energy (eV)
C^+	$2s^2 2p\,^2P^o$	0.00
	$2s2p^2\,^4P$	5.33
	$2s2p^2\,^2D$	9.29
	$2s2p^2\,^2S$	11.96
	$2s2p^2\,^2P$	13.72
	$2s^2 3s\,^2S$	14.45
C^{2+}	$2s^2\,^1S$	24.38
	$2s2p\,^3P^o$	30.88

2.2. Achievable TES resolution

2.2.1. Available (centre-of-mass) collision energy for inelastic reactions. Considering the inelastic collision of a projectile ion p (mass m_p, kinetic energy E_p in the laboratory system) with a target molecule t at rest in the laboratory system (mass m_t; inelastic energy defect Q),
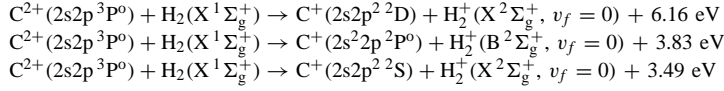
$$p + t \rightarrow p' + t' + Q \tag{1}$$

the kinetic energy for inelastic reactions available in the centre-of-mass system will be given by

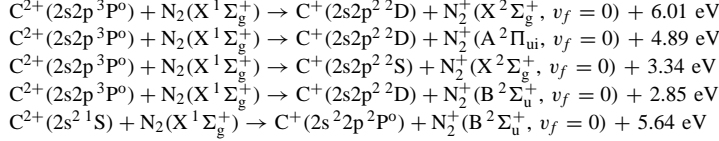$$E_{cm} = E_p m_t / (m_p + m_t) \tag{2}$$

with unprimed and primed quantities referring to pre- and postcollision particles, respectively.

Table 3. (*a*) Observed SEC reaction channels for C^{2+}–H_2 collisions. (*b*) Observed SEC reaction channels for C^{2+}–N_2 collisions. (*c*) Observed SEC reaction channels for C^{2+}–O_2 collisions. (*d*) Observed SEC reaction channels for C^{2+}–CO collisions.
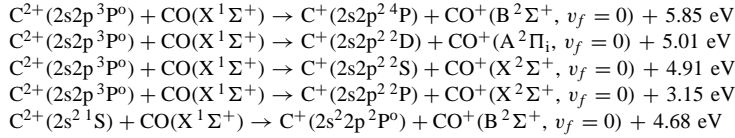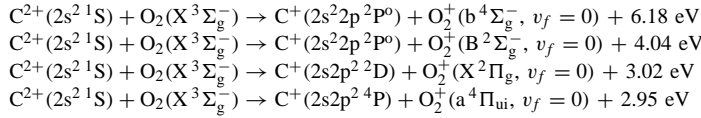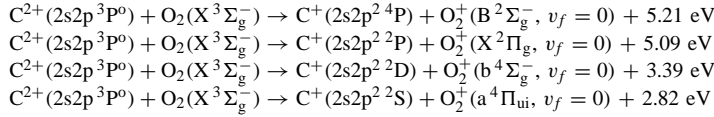
(*a*) Observed SEC reaction channels for C^{2+}–H_2 collisions.
$C^{2+}(2s2p\,^3P^o) + H_2(X\,^1\Sigma_g^+) \rightarrow C^+(2s2p^2\,^2D) + H_2^+(X\,^2\Sigma_g^+, v_f = 0) + 6.16$ eV
$C^{2+}(2s2p\,^3P^o) + H_2(X\,^1\Sigma_g^+) \rightarrow C^+(2s^22p\,^2P^o) + H_2^+(B\,^2\Sigma_g^+, v_f = 0) + 3.83$ eV
$C^{2+}(2s2p\,^3P^o) + H_2(X\,^1\Sigma_g^+) \rightarrow C^+(2s2p^2\,^2S) + H_2^+(X\,^2\Sigma_g^+, v_f = 0) + 3.49$ eV
(*b*) Observed SEC reaction channels for C^{2+}–N_2 collisions.
$C^{2+}(2s2p\,^3P^o) + N_2(X\,^1\Sigma_g^+) \rightarrow C^+(2s2p^2\,^2D) + N_2^+(X\,^2\Sigma_g^+, v_f = 0) + 6.01$ eV
$C^{2+}(2s2p\,^3P^o) + N_2(X\,^1\Sigma_g^+) \rightarrow C^+(2s2p^2\,^2D) + N_2^+(A\,^2\Pi_{ui}, v_f = 0) + 4.89$ eV
$C^{2+}(2s2p\,^3P^o) + N_2(X\,^1\Sigma_g^+) \rightarrow C^+(2s2p^2\,^2S) + N_2^+(X\,^2\Sigma_g^+, v_f = 0) + 3.34$ eV
$C^{2+}(2s2p\,^3P^o) + N_2(X\,^1\Sigma_g^+) \rightarrow C^+(2s2p^2\,^2D) + N_2^+(B\,^2\Sigma_u^+, v_f = 0) + 2.85$ eV
$C^{2+}(2s^2\,^1S) + N_2(X\,^1\Sigma_g^+) \rightarrow C^+(2s^22p\,^2P^o) + N_2^+(B\,^2\Sigma_u^+, v_f = 0) + 5.64$ eV
(*c*) Observed SEC reaction channels for C^{2+}–CO collisions.
$C^{2+}(2s2p\,^3P^o) + CO(X\,^1\Sigma^+) \rightarrow C^+(2s2p^2\,^4P) + CO^+(B\,^2\Sigma^+, v_f = 0) + 5.85$ eV
$C^{2+}(2s2p\,^3P^o) + CO(X\,^1\Sigma^+) \rightarrow C^+(2s2p^2\,^2D) + CO^+(A\,^2\Pi_i, v_f = 0) + 5.01$ eV
$C^{2+}(2s2p\,^3P^o) + CO(X\,^1\Sigma^+) \rightarrow C^+(2s2p^2\,^2S) + CO^+(X\,^2\Sigma^+, v_f = 0) + 4.91$ eV
$C^{2+}(2s2p\,^3P^o) + CO(X\,^1\Sigma^+) \rightarrow C^+(2s2p^2\,^2P) + CO^+(X\,^2\Sigma^+, v_f = 0) + 3.15$ eV
$C^{2+}(2s^2\,^1S) + CO(X\,^1\Sigma^+) \rightarrow C^+(2s^22p\,^2P^o) + CO^+(B\,^2\Sigma^+, v_f = 0) + 4.68$ eV
(*d*) Observed SEC reaction channels for C^{2+}–O_2 collisions.
$C^{2+}(2s2p\,^3P^o) + O_2(X\,^3\Sigma_g^-) \rightarrow C^+(2s2p^2\,^4P) + O_2^+(B\,^2\Sigma_g^-, v_f = 0) + 5.21$ eV
$C^{2+}(2s2p\,^3P^o) + O_2(X\,^3\Sigma_g^-) \rightarrow C^+(2s2p^2\,^2P) + O_2^+(X\,^2\Pi_g, v_f = 0) + 5.09$ eV
$C^{2+}(2s2p\,^3P^o) + O_2(X\,^3\Sigma_g^-) \rightarrow C^+(2s2p^2\,^2D) + O_2^+(b\,^4\Sigma_g^-, v_f = 0) + 3.39$ eV
$C^{2+}(2s2p\,^3P^o) + O_2(X\,^3\Sigma_g^-) \rightarrow C^+(2s2p^2\,^2S) + O_2^+(a\,^4\Pi_{ui}, v_f = 0) + 2.82$ eV
$C^{2+}(2s^2\,^1S) + O_2(X\,^3\Sigma_g^-) \rightarrow C^+(2s^22p\,^2P^o) + O_2^+(b\,^4\Sigma_g^-, v_f = 0) + 6.18$ eV
$C^{2+}(2s^2\,^1S) + O_2(X\,^3\Sigma_g^-) \rightarrow C^+(2s^22p\,^2P^o) + O_2^+(B\,^2\Sigma_g^-, v_f = 0) + 4.04$ eV
$C^{2+}(2s^2\,^1S) + O_2(X\,^3\Sigma_g^-) \rightarrow C^+(2s2p^2\,^2D) + O_2^+(X\,^2\Pi_g, v_f = 0) + 3.02$ eV
$C^{2+}(2s^2\,^1S) + O_2(X\,^3\Sigma_g^-) \rightarrow C^+(2s2p^2\,^4P) + O_2^+(a\,^4\Pi_{ui}, v_f = 0) + 2.95$ eV

2.2.2. Relation between inelastic reaction energy defect Q and projectile energy loss/gain. For an inelastic collision with reaction energy defect Q and small projectile scattering angle ϑ we obtain a translational energy loss/gain $\Delta E = E_p - E_p'$ (Fukuroda *et al* 1989):

$$\Delta E = Q - \frac{m_p}{m_t}\left(\frac{Q^2}{4E_p} + E_p\vartheta^2\right). \tag{3}$$

2.2.3. Influence of the projectile acceptance angle $\Delta\vartheta$ on TES resolution. Equation (3) permits a rough estimate of the contribution δ_ϑ from the effective projectile acceptance angle $\Delta\vartheta$ on the achievable TES resolution, if Q is much smaller than the projectile energy E_p:

$$\delta_\vartheta \approx \Delta\vartheta^2 E_p m_p/m_t. \tag{4}$$

For all TES measurements to be presented, careful checks by varying ϑ around $0°$ have been made to assure that $\Delta\vartheta$ was indeed sufficiently large to avoid any discrimination of essential TES features (cf Jellen-Wutte *et al* 1985).
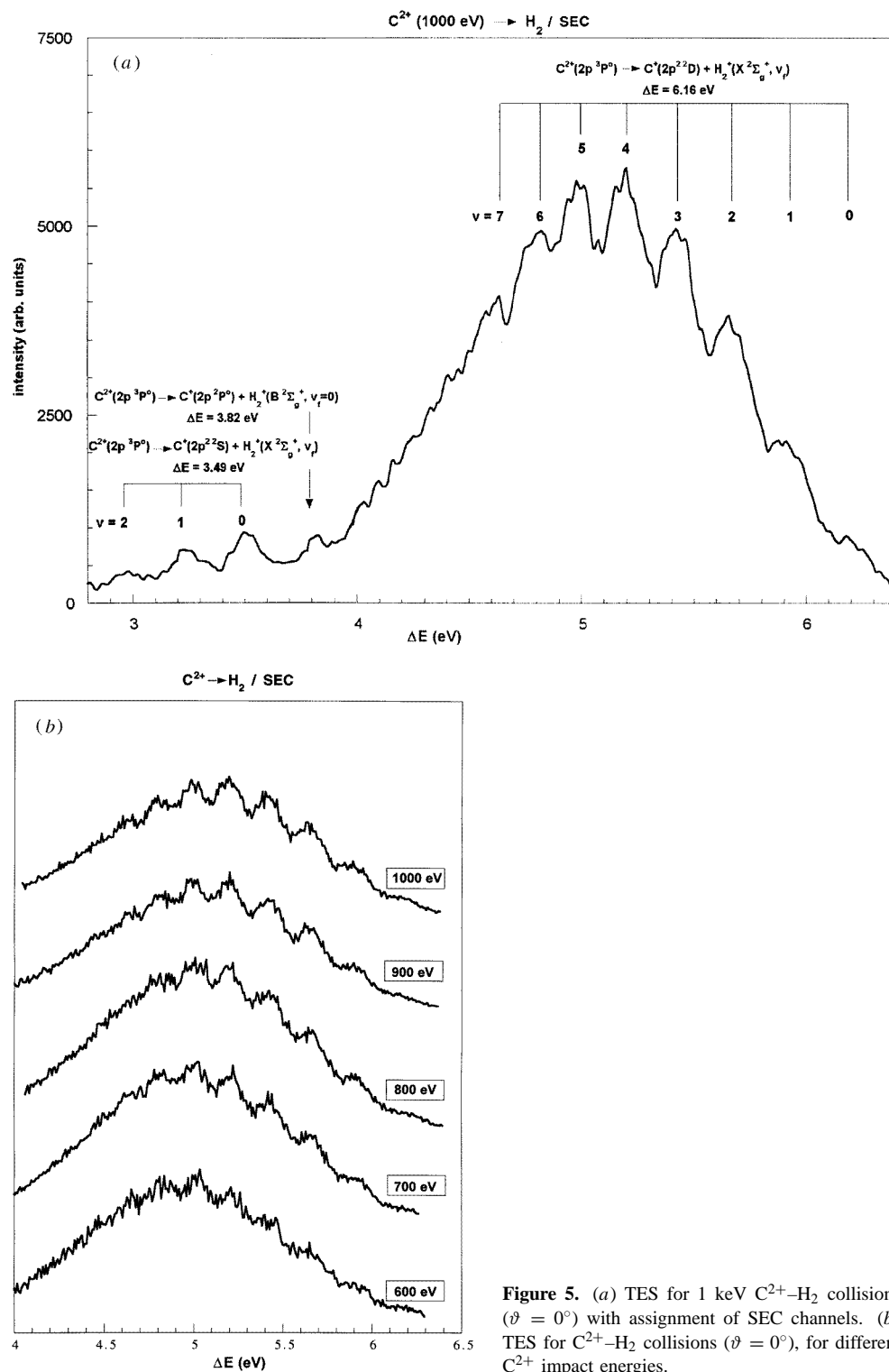
Figure 5. (*a*) TES for 1 keV C^{2+}–H_2 collisions ($\vartheta = 0°$) with assignment of SEC channels. (*b*) TES for C^{2+}–H_2 collisions ($\vartheta = 0°$), for different C^{2+} impact energies.
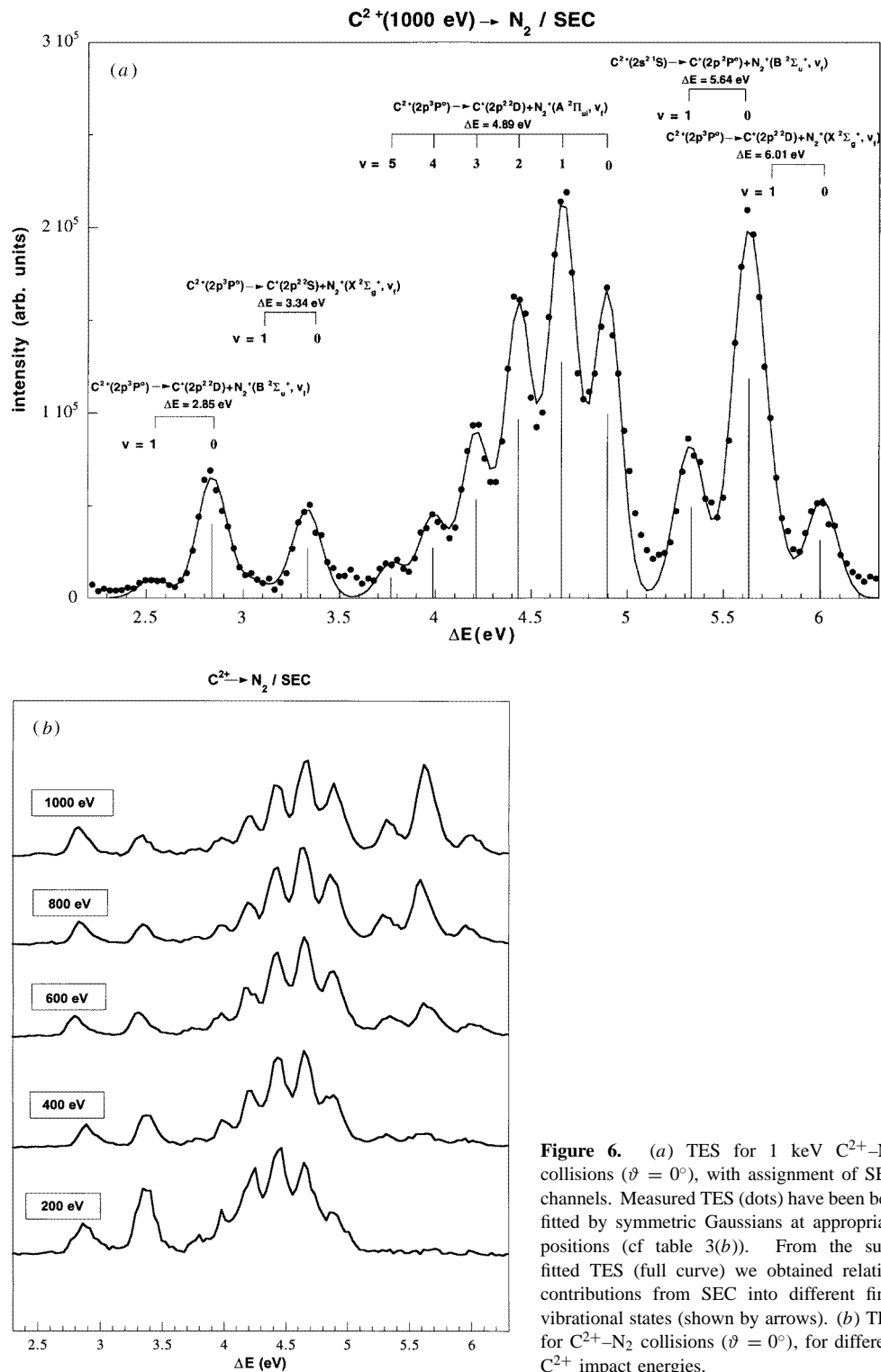
Figure 6. (*a*) TES for 1 keV C^{2+}–N_2 collisions ($\vartheta = 0°$), with assignment of SEC channels. Measured TES (dots) have been best fitted by symmetric Gaussians at appropriate positions (cf table 3(*b*)). From the such fitted TES (full curve) we obtained relative contributions from SEC into different final vibrational states (shown by arrows). (*b*) TES for C^{2+}–N_2 collisions ($\vartheta = 0°$), for different C^{2+} impact energies.

$C^{2+}(ms) + N_2 \rightarrow C^+(^2D) + N_2^+(A^2\Pi_{ul})$

Experimental Data and MLZ - Calculations
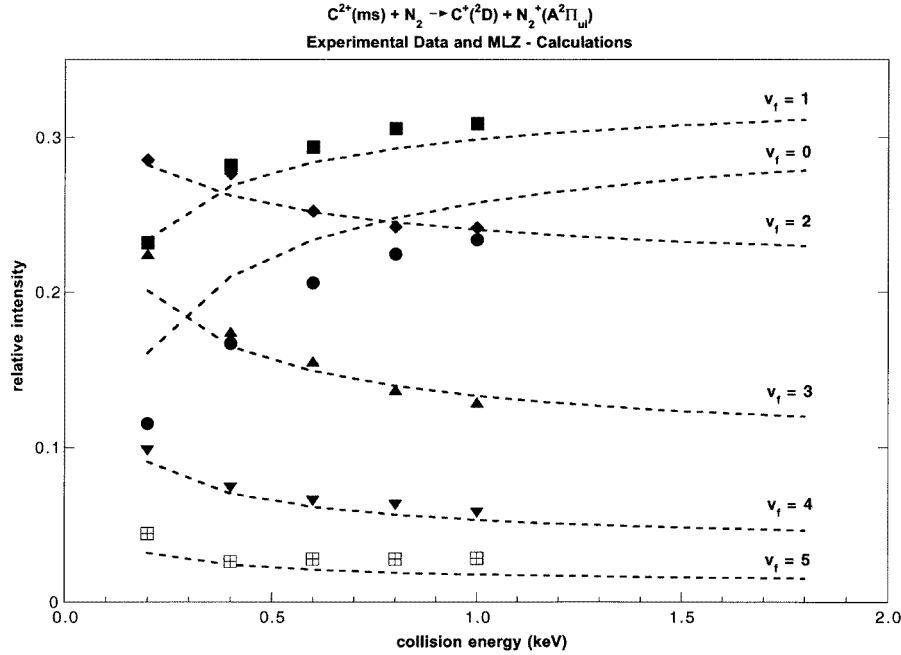
Figure 7. Comparison of measured (full circles, squares, diamonds, etc refer to $v_f = 0, 1, 2$, etc, respectively) with calculated relative contributions by final vibrational states in the central SEC group of figure 6(*a*) versus impact energy (for further explanation cf text).

2.2.4. Influence of the target gas temperature on TES resolution. At forward scattering ($\vartheta \approx 0$) the kinetic energy of scattering projectiles is broadened because of a non-zero target particle temperature T_t, resulting in a TES peak FWHM δ_T (Fukuroda *et al* 1989):

$$\delta_T = 2Q\sqrt{\ln 2 \frac{m_p}{m_t} \frac{kT_t}{E_p}}. \tag{5}$$

If primary ions after leaving the monochromator already feature a nominal kinetic energy width δ_p, the analyser energy width δ_A, finite acceptance angle Δ_ϑ and target temperature T_t add up to a total effective energy width δE_p of the inelastically scattered projectiles:

$$\delta E_p \approx [\delta_p{}^2 + \delta_A{}^2 + \delta_\vartheta{}^2 + \delta_T{}^2]^{1/2}. \tag{6}$$

Unfortunately, Δ_ϑ cannot be determined in a straightforward manner because of the *a priori* unknown influence of the acceleration and deceleration lenses which are sandwiching the collision cell.

Figure 2 shows a TES as measured in forward scattering ($\vartheta = 0°$) of 1 keV He^+ on H_2. The two essential peaks have been best-fitted to symmetric Gaussians of appropriate FWHM.

The analyser geometry delivers a kinetic energy resolution $\delta_A \approx 4.5 \times 10^{-3}$ q.e. U_p. The elastic He^+ peak (at zero on the kinetic energy scale) is only broadened due to contributions by δ_A and the influence of the monochromator (once more δ_A). For the given pass energies of 9 eV this causes a FWHM of 59 meV, in rather good agreement with the measured FWHM $\delta E_p \approx 60$ meV (cf figure 2). For the inelastically scattered projectiles, however, in addition, the finite acceptance angle and target temperature have to be taken into account, as is apparent from the small peak at $\Delta E \approx 0.52$ eV ($v' = 0 \rightarrow v'' = 1$ vibrational
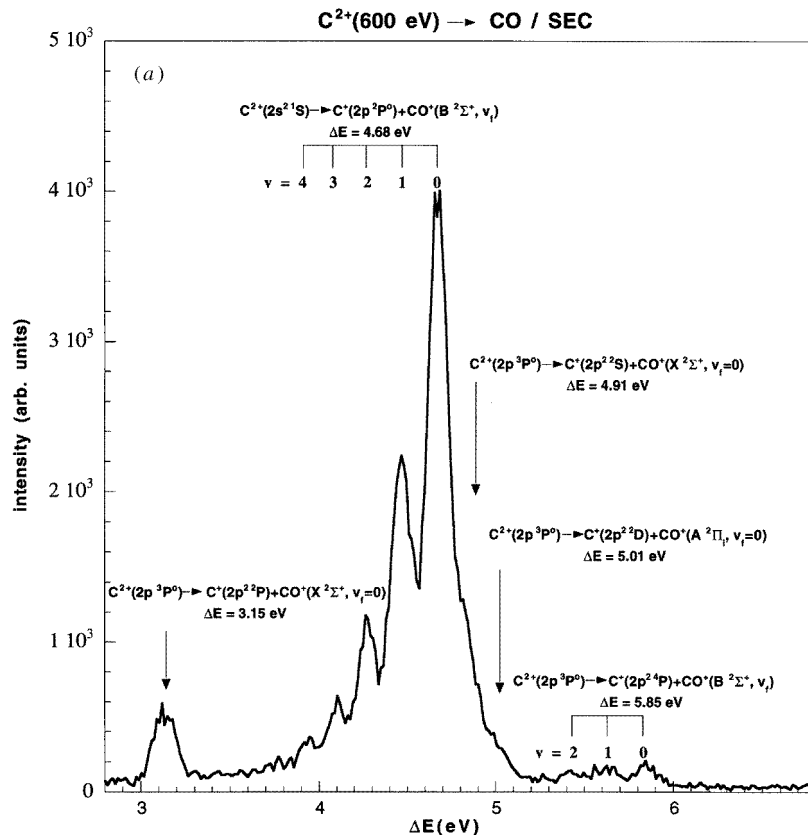
Figure 8. (*a*) TES for 0, 6 keV C^{2+}–CO collisions ($\vartheta = 0°$), with assignment of SEC channels. (*b*) TES for C^{2+}–CO collisions ($\vartheta = 0°$) for different C^{2+} impact energies.

excitation of H_2, cf table 1) with a δE_p of 75 meV. With $m_p/m_t = 2$, target molecules at room temperature and the reaction energy defect $Q = 0.52$ eV, equation (5) predicts a rather small 'thermal' broadening contribution $\delta_T \approx 6$ meV, which cannot be responsible for the considerably larger FWHM apparent from figure 2. An additional broadening of about 45 meV probably results from the contribution δ_ϑ which according to equation (4) corresponds to an effective acceptance angle $\Delta\vartheta \leqslant 0.3°$. From this analysis we conclude that the deceleration and acceleration lenses in front of and behind the collision cell are of no significant influence on the effective TES acceptance angle. Rather, the latter is determined by the geometry of the monochromator exit and the analyser entrance apertures. The achievable resolution is also seen from figure 3 for impact of Ne^+ on N_2. Symmetrically to the central elastic peak small inelastic peaks belong to collisional excitation ($j = \frac{3}{2} \to \frac{1}{2}$; endothermic side, denoted 'ex') and de-excitation ($j = \frac{3}{2} \leftarrow \frac{1}{2}$; exothermic side, denoted 'dx') of the Ne^+ $2p^5\,^2P^o_{3/2}$ ground and the Ne^+ $2p^5\,^2P^o_{1/2}$ metastable state, respectively, corresponding to energy defects $\Delta E = \pm 97$ meV (Bashkin and Stoner 1975).

A small inelastic peak further down on the endothermic side (denoted 'di/01') demonstrates the first vibrational excitation of N_2 (see table 1), similar to $He^+ \to H_2$ (see figure 2).
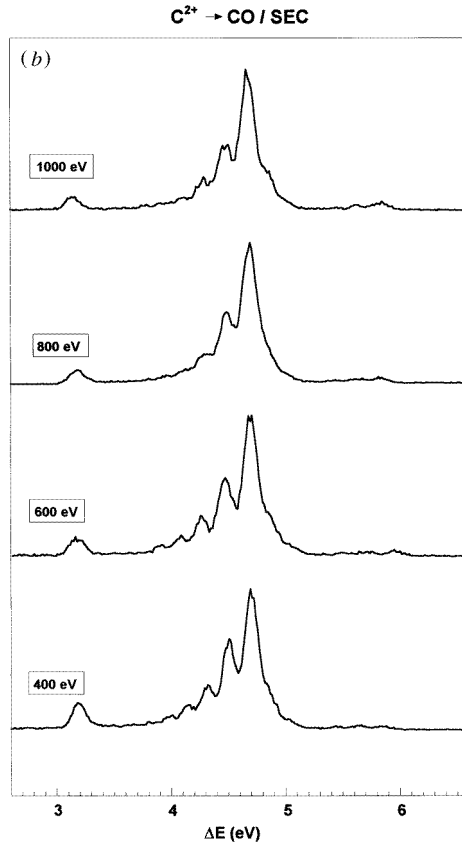
Figure 8. (Continued)

Finally, the performance of our instrument is shown for SEC by doubly charged C^{2+} ions from Ar, which system has already been studied by Unterreiter *et al* (1991) and Greenwood *et al* (1996):

$$C^{2+}(2s^2\,{}^1S) + Ar \rightarrow C^+(n, \ell) + Ar^+ + Q \tag{7a}$$

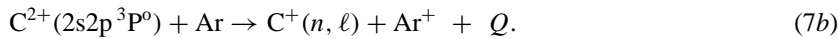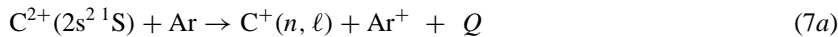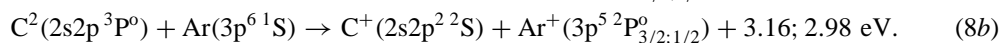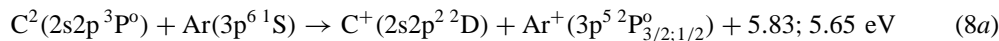$$C^{2+}(2s2p\,{}^3P^o) + Ar \rightarrow C^+(n, \ell) + Ar^+ + Q. \tag{7b}$$

Table 2 shows configurations and excitation energies of the ground state and the five lowest excited states of C^+, and ionization energies for reaching the C^{2+} ground state and the C^{2+} metastable state from the C^+ ground state, respectively (all data are compiled from Bashkin and Stoner (1975)).

For all these states fine-structure splittings (if present) are typically below 10 meV and thus cannot contribute appreciably to TES broadening. Ionization from the Ar neutral ground state into the $3p^5\,{}^2P^o_{3/2}$ and the $3p^5\,{}^2P^o_{1/2}$ ion states requires 15.76 and 15.94 eV, respectively (Bashkin and Stoner 1978), from which values the following reaction energy defects Q for particular initial-to-final state selective SEC processes by ground state and metastable C^{2+} projectiles can be derived.

$$C^2(2s2p\,{}^3P^o) + Ar(3p^6\,{}^1S) \rightarrow C^+(2s2p^2\,{}^2D) + Ar^+(3p^5\,{}^2P^o_{3/2;1/2}) + 5.83;\ 5.65\ eV \tag{8a}$$

$$C^2(2s2p\,{}^3P^o) + Ar(3p^6\,{}^1S) \rightarrow C^+(2s2p^2\,{}^2S) + Ar^+(3p^5\,{}^2P^o_{3/2;1/2}) + 3.16;\ 2.98\ eV. \tag{8b}$$

Corresponding TES shown in figure 4 have been obtained with C^{2+} ions from an ECR ion source (see above), for which the metastable $C^{2+}(2s2p\,^3P^o)$ ion beam fraction was typically 30–50% (Brazuk *et al* 1984, Winter 1995, Greenwood *et al* 1996). The clear double structure of TES peaks reflects the 178 meV fine-structure splitting of the two lowest Ar^+ states (see above), with their statistical weights explaining the intensity ratio of about 2:1 as apparent from figure 4.

To assure a correct energy defect assignment for all peaks in the rather rich TES for SEC from the molecular targets (see below), we have performed all related TES measurements at fixed projectile energies by rapid switching between the chosen molecular target gas and Ne, using the well established TES features for SEC in C^{2+}–Ne collisions (Greenwood *et al* 1996).

3. Presentation data for final vibrational state selective SEC by ground state and metastable C^{2+} from H_2, N_2, O_2 and CO

From the vibrational excitation and first ionization energies given in table 1, and the excitation energies for C^+ final projectile states in table 2 we have derived energy defects for various SEC channels involving ground state and metastable C^{2+} primary ions, and target molecules H_2, N_2, O_2 and CO, respectively. These energy defects (for $v_f = 0$) are given in table 3(a)–(d) for all TES features actually observed (see below). Probable SEC channels involve energy defects within the so-called 'reaction energy window', which can be derived from Landau–Zener calculations with empirically obtained coupling matrix elements (Kimura *et al* 1984, Taulbjerg 1986). For projectile charge $q = 2$ the situation of the centre of the reaction energy window and its width depend only on the target ionization energy and projectile velocity. The centre of the reaction window shifts towards smaller exothermic energy defect for smaller target ionization energy and/or lower projectile velocity. For SEC from H_2 various model calculations showed that for 1 keV C^{2+} impact energy the reaction energy window is centred near $\Delta E = 4.4$ eV and features a typical FWHM of 1.2 eV. If the impact energy is decreased from 1 to 0.2 keV, the window centre shifts by about 0.5 eV. We therefore expect the most probable SEC channels with reaction energy defects between 3 and 6 eV, if final projectile states with the appropriate binding energies are actually available.

The TES for 1 keV C^{2+} impact on H_2 in figure 5(a) demonstrates that the by-far dominant SEC channels correspond to the first reactions plotted in table 3(a), for which final vibrational states with increasing excitation fit gradually better into the above-given reaction energy window. Other possible SEC channels which do not fall into the reaction energy window are strongly suppressed. Figure 5(b) shows TES for SEC from H_2 for different C^{2+} impact energies, from which the increasing relative importance of higher final vibrational states with decreasing impact energy can be seen, in accordance with the above-explained behaviour of the reaction energy window. Unfortunately, the resolution of these TES measurements is not high enough to permit a really unambiguous evaluation of the relative importance of different final vibrational states. This is caused by a relatively large thermal broadening because of the high projectile-to-target mass ratio involved (cf equation (5) in section 2.2 and discussion in Fukuroda *et al* (1989) for the comparable case of Ne^{2+}–H_2).

A TES for 1 keV C^{2+}–N_2 collisions is shown in figure 6(a). Its resolution is better than for C^{2+}–H_2 (cf figure 5(a)), because of a considerably smaller thermal broadening (see above, and measurements for Ne^{2+}–N_2 by Okuno *et al* (1989)). Figure 6(b) shows TES for different projectile impact energies which clearly demonstrate the related shift of the respective reaction energy window. This case is similar to SEC from H_2 because of
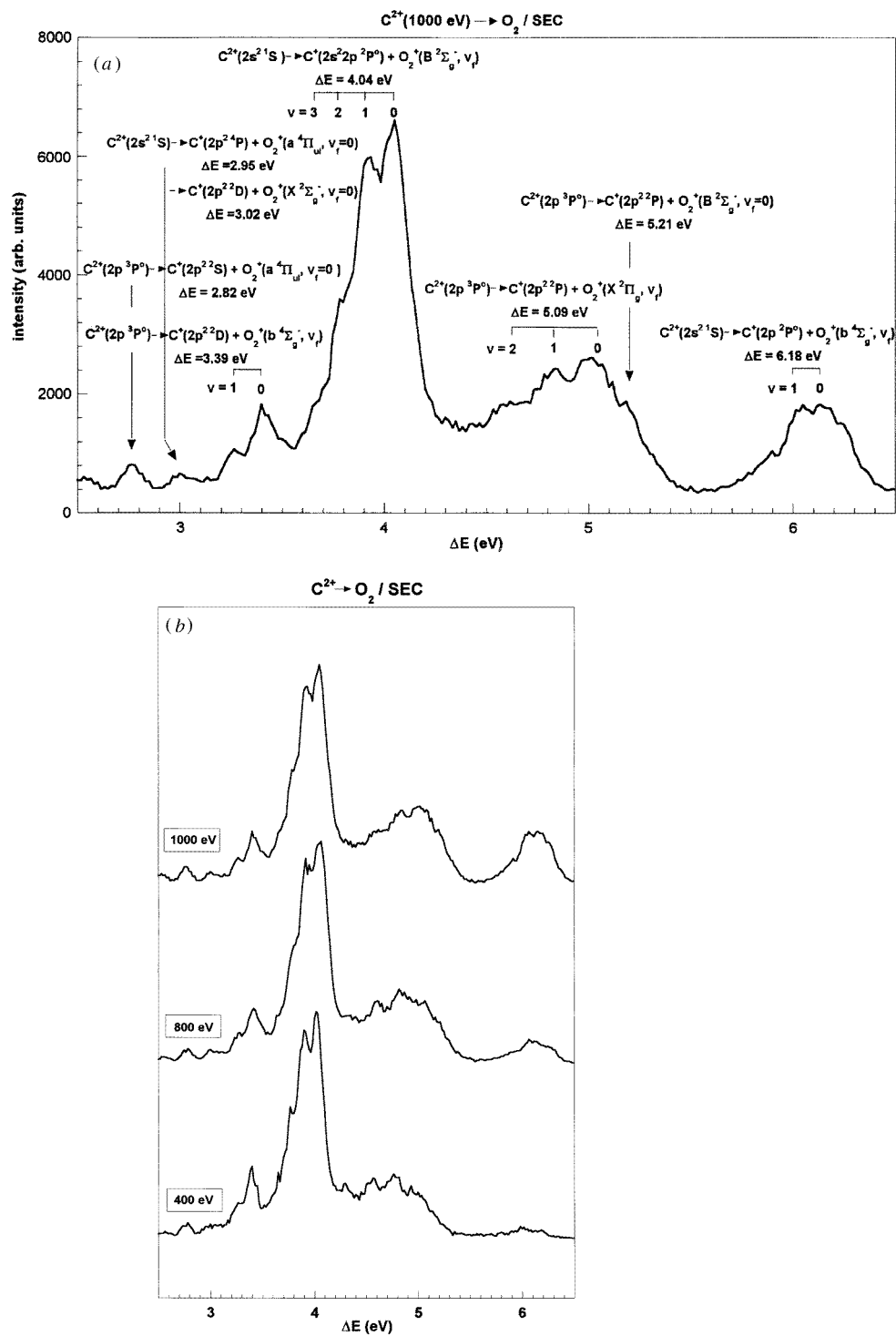
C^{2+}(1000 eV) $\rightarrow O_2$ / SEC

$C^{2+}(2s^2\,{}^1S) \rightarrow C^+(2s^2 2p\,{}^2P^o) + O_2^+(B\,{}^2\Sigma_g^-, v_f)$

$\Delta E = 4.04$ eV

v = 3 2 1 0

$C^{2+}(2s^2\,{}^1S) \rightarrow C^+(2p^2\,{}^4P) + O_2^+(a\,{}^4\Pi_u, v_f=0)$

$\Delta E = 2.95$ eV

$\rightarrow C^+(2p^2\,{}^2D) + O_2^+(X\,{}^2\Sigma_g^-, v_f=0)$

$\Delta E = 3.02$ eV

$C^{2+}(2p\,{}^3P^o) \rightarrow C^+(2p^2\,{}^2P) + O_2^+(B\,{}^2\Sigma_g^-, v_f=0)$

$\Delta E = 5.21$ eV

$C^{2+}(2p\,{}^3P^o) \rightarrow C^+(2p^2\,{}^2S) + O_2^+(a\,{}^4\Pi_u, v_f=0)$

$\Delta E = 2.82$ eV

$C^{2+}(2p\,{}^3P^o) \rightarrow C^+(2p^2\,{}^2P) + O_2^+(X\,{}^2\Pi_g, v_f)$

$\Delta E = 5.09$ eV

v = 2 1 0

$C^{2+}(2p\,{}^3P^o) \rightarrow C^+(2p^2\,{}^2D) + O_2^+(b\,{}^4\Sigma_g^-, v_f)$

$\Delta E = 3.39$ eV

v = 1 0

$C^{2+}(2s^2\,{}^1S) \rightarrow C^+(2p\,{}^2P^o) + O_2^+(b\,{}^4\Sigma_g^-, v_f)$

$\Delta E = 6.18$ eV

v = 1 0

intensity (arb. units)

ΔE (eV)

(a)

(b)

$C^{2+} \rightarrow O_2$ / SEC

1000 eV

800 eV

400 eV

ΔE (eV)

Figure 9. (*a*) TES for 1 keV C^{2+}–O_2 collisions ($\vartheta = 0°$), with assignment of SEC channels. (*b*) TES for C^{2+}–O_2 collisions ($\vartheta = 0°$) for different C^{2+} impact energies.

the comparably large ionization energies of H_2 and N_2. Features appearing in the TES of figure 6(a) are related to the reaction channels listed in table 3(b). In contrast to SEC from H_2, however, we also find one important SEC channel starting from the C^{2+} ground state. The TES shown in figure 6(a) has been best fitted to an ensemble of symmetric Gaussians positioned at the appropriate reaction energy defects. The relative importance of channels involving different C^{2+} primary ion species cannot be determined because of the not precisely known primary ion metastable fraction. The dominant feature inside the reaction window covers final vibrational states starting with

$$C^{2+}(2s2p\,^3P^o) + N_2(X\,^1\Sigma_g^+) \rightarrow C^+(2s2p^2\,^2D) + N_2^+(A\,^2\Pi_{ui}, v_f = 0) + 4.89\ \text{eV} \qquad (9)$$
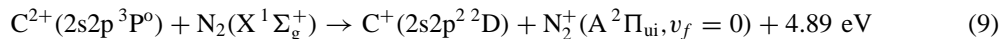
Because of a sufficiently high TES resolution the relative contributions from different final vibrational states could be evaluated. The thus obtained data (shown by arrows in figure 6(a)) have been compared with results from multichannel Landau–Zener calculations (method as given by Salop and Olson (1976), Kimura *et al* (1984)), which have been performed in the following way. The probability p for a diabatic transition at the crossing of two potential energy curves of the collisional quasimolecule (in the present case (C–$N_2)^{2+}$) is given by

$$p = \exp\left(-\frac{2\pi H_{12}^2 FCF}{v_r \Delta F}\right) \qquad (10)$$

where v_r is the relative velocity of the collision partners at the crossing point, H_{12} is the respective coupling matrix element (i.e. one half of the adiabatic splitting) at the respective curve crossing, FCF is the appropriate Franck–Condon factor (Halmann and Laulicht 1965, Gilmore *et al* 1992), and ΔF is the difference in slopes of the diabatic potential energy curves at the respective crossing. For an isolated crossing the total probability for electron transfer is then $P = 2p(1 - p)$. For multichannel crossings a more general expression gives probabilities P_i for particular final vibrational levels i within a group of SEC channels, if couplings between adjacent exit channels are neglected (Salop and Olson 1976).

Under these assumptions we have calculated for different impact energies the relative importance of SEC into different final vibrational states of the reaction channel according to equation (9). Comparison of the results with corresponding experimental data from figure 6(a) shows a quite satisfactory agreement (see figure 7).

TES for C^{2+}–CO collisions are shown in figures 8(a), (b), and for C^{2+}–O_2 collisions in figures 9(a), (b). For both collision systems all prominent TES features have been identified and listed in tables 3(c) and 3(d), respectively. The relative importance of the different SEC channels and their variation with impact energy is again well understood from the corresponding reaction energy windows (see above).

4. Summary and conclusions

We have performed ion translational energy spectroscopy for single-electron capture in collisions of ground state and metastable C^{2+} (impact energy $\leqslant$ 1 keV) with simple target molecules H_2, N_2, O_2 and CO. The ion kinetic energy resolution achieved in these measurements was sufficiently high (typically $\leqslant$ 200 meV) to permit clear distinction between the first final vibrational states for SEC channels between given electronic states. This constitutes an important step beyond former TES studies on these collision systems, which have been performed with considerably lower kinetic energy resolution (Unterreiter *et al* 1991, Burns *et al* 1997). Furthermore, the high TES resolution permitted a clear distinction between channels starting from ground state and metastable primary ions

respectively, which otherwise can only be achieved by state-selective primary ion beam preparation (Huber *et al* 1984, Greenwood *et al* 1996). Interpretation of our results considers the energy situation and width of the respective reaction windows, which are derived from Landau–Zener calculations with empirically determined coupling matrix elements. For the main reaction channel in C^{2+}–N_2 collisions, multichannel Landau–Zener calculations taking into account the appropriate Franck–Condon factors could satisfactorily reproduce the measured final vibrational state distribution. The present investigations are also useful for explaining impact energy dependences of corresponding total SEC cross sections, which in turn are important for various plasma-related applications in, for example, astrophysics, magnetic fusion research and plasma chemistry.

Acknowledgments

References

Bashkin S and Stoner J O Jr 1975 *Atomic Energy Levels and Grotrian Diagrams* vol 1 (Amsterdam: North-Holland)
——1978 *Atomic Energy Levels and Grotrian Diagrams* vol 2 (Amsterdam: North-Holland)
Brazuk A, Dijkkamp D, Drentje A G, de Heer F J and Winter H P 1984 *J. Phys. B: At. Mol. Phys.* **17** 2489
Brenton A G 1995 *J. Mass Spectrom.* **30** 657
Burns D, Greenwood J B, Bajajova K R, McCullough R W, Geddes J and Gilbody H B 1997 *J. Phys. B: At. Mol. Opt. Phys.* **30** 1531
Farnik M, Herman Z, Ruhaltinger T, Toennies J P and Wang R G 1993 *Chem. Phys. Lett.* **206** 376
Fukuroda A, Kobayashi N and Kaneko Y 1989 *J. Phys. B: At. Mol. Opt. Phys.* **22** 3457
Gilbody H B 1994 *Adv. At. Mol. Opt. Phys.* **32** 149
Gilmore F R, Laher R R and Espy P J 1992 *J Phys. Chem. Ref. Data* **21** 1005
Gislason E A and Parlant G 1987 *Comment. At. Mol. Phys* **19** 157
Greenwood J B, Burns D, McCullough R W, Geddes J and Gilbody H P 1996 *J. Phys. B: At. Mol. Opt. Phys.* **29** 5867
Halmann M and Laulicht I 1965 *J. Chem. Phys.* **43** 1503
Heil T G 1987 *Nucl. Instrum. Methods* B **24** 222
Herzberg G 1950 *Molecular Spectra and Molecular Structure I: Spectra of Diatomic Molecules* 2nd edn (New York: Van Nostrand)
Hodge W L, Goldberger A L, Vedder M and Pollack E 1977 *Phys. Rev.* A **16** 2360
Hoekstra R, de Heer F J and Morgenstern R 1991 *Z. Phys.* D **21** 81
Huber K P and Herzberg G 1979 *Constants of Diatomic Molecules* (Princeton, NJ: Van Nostrand-Reinhold)
Huber B A and Kahlert H-J 1985 *J. Phys. B: At. Mol. Phys.* **18** 491
Huber B A, Kahlert H-J and Wiesemann K 1984 *J. Phys. B: At. Mol. Phys.* **17** 2883
Itoh Y, Nakamura T, Kobayashi N and Kaneko Y 1983 *J. Phys. Soc. Japan* **52** 1091
Janev R K (ed) 1995 *Atomic and Molecular Processes in Fusion Edge Plasmas* (New York: Plenum)
Janev R K and Winter H P 1985 *Phys. Rep* **117** 265
Janev R K, Winter H P and Fritsch W 1995 *Atomic and Molecular Processes in Fusion Edge Plasmas* ed R K Janev (New York: Plenum) ch 13
Jellen-Wutte U, Schweinzer J, Vanek W and Winter H P 1985 *J. Phys. B: At. Mol. Phys.* **18** L779
Kahlert H-J, Huber B A and Wiesemann K 1983 *J. Phys. B: At. Mol. Phys.* **16** 449
Kimura M *et al* 1984 *J. Phys. Soc. Japan* **53** 2224
Kobayashi N, Itoh Y and Kaneko Y 1978 *J. Phys. Soc. Japan* **45** 617
——1979 *J. Phys. Soc. Japan* **46** 208
Leitner M, Wutte D, Brandstötter J, Aumayr F and Winter H P 1994 *Rev. Sci. Instrum.* **65** 1091
Linder F 1980 *Electronic and Atomic Collisions* ed N Oda and K Takayanagi (Amsterdam: North-Holland) p 535

Matsuo T, Kobayashi N and Kaneko Y 1982 *J. Phys. Soc. Japan* **51** 1558

Nakamura T, Kobayashi N and Kaneko Y 1986 *J. Phys. Soc. Japan* **55** 3831

Neidner-Schatteburg G and Toennies J P 1992 Proton energy loss spectroscopy as a state-to-state probe of molecular dynamics *State-Selected and State-to-State Ion–Molecule Reaction Dynamics, Part 1. Experiment* ed C-Y Ng and M Baer (New York: Wiley)

Niehaus A 1986 *J. Phys. B: At. Mol. Phys.* **19** 2925

Okuno K, Fukuroda A, Kobayashi N and Kaneko Y 1989 *J. Phys. Soc. Japan* **58** 1590

Salop A and Olson R E 1976 *Phys. Rev.* A **13** 1312

Sato Y and Moore J H 1979 *Phys. Rev.* A **19** 495

Schweinzer J and Winter H P 1989 *J. Phys. B: At. Mol. Opt. Phys.* **22** 893

Taulbjerg K 1986 *J. Phys. B: At. Mol. Phys.* **19** L367

Unterreiter E, Schweinzer J and Winter H P 1991 *J. Phys. B: At. Mol. Opt. Phys.* **24** 1003

Wilkie F G, McCullough R W and Gilbody H B 1986 *J. Phys. B: At. Mol. Phys.* **19** 239

Winter H P 1995 *J. Phys. Chem.* **99** 15 448